Optical Flow based Deformable Volume Registration using a novel Second-Order Regularization Prior

Saša Grbić [a] and Martin Urschler [a] and Thomas Pock [a] and Horst Bischof [a]

[a] Institute for Computer Graphics & Vision, Graz University of Technology, Austria

ABSTRACT

Nonlinear image registration is an initial step for a large number of medical image analysis applications. Optical flow based intensity registration is often used for dealing with intra-modality applications involving motion differences. In this work we present an energy functional which uses a novel, second-order regularization prior of the displacement field. Compared to other methods our scheme is robust to non-Gaussian noise and does not penalize locally affine deformation fields in homogeneous areas. We propose an efficient and stable numerical scheme to find the minimizer of the presented energy. We implemented our algorithm using modern consumer graphics processing units and thereby increased the execution performance dramatically. We further show experimental evaluations on clinical CT thorax data sets at different breathing states and on dynamic 4D CT cardiac data sets.

Keywords: Nonlinear image registration

1. INTRODUCTION

Nonlinear (deformable) registration of data sets acquired at different points in time is an important research topic in medical image analysis. Image sequences of soft tissue organs like lung or liver during breathing or the beating heart often require registration algorithms to compensate for motion differences. Surveys on nonlinear registration techniques in medical imaging can be found in Maintz and Viergever[1] or Crum *et al.*.[2] In literature, one distinguishes feature- and intensity based nonlinear registration methods. Intensity based methods[3, 4] are often favored since they make use of the entire image information, however, they come at the cost of a high computational effort.

Most of the optical flow based approaches penalize first order derivatives of the displacement field in their regularization term. This induces a bias towards certain deformation fields in homogeneous areas. Quadratic regularization[5] favors smooth fields, but also tends to smooth over discontinuities in the deformation field. Total variation regularization[6] favors piecewise constant solutions in untextured areas. Deformable soft tissue behaves locally in an elastic manner, leaving the physical justification of total variation models questionable. Despite nonlinearities and anisotropy, stretching of soft tissue is locally smooth and not piecewise constant. In a local neighborhood this can be approximated by an affine deformation model. First order total variation regularization penalizes such deviations since they differ from piecewise constant solutions. In this work we investigate second order regularization, using a novel second order regularization prior, as an alternative for modeling elastic soft tissue behavior. This is in contrast to elastic registration,[3] which approximates locally affine deformations with a combination of first order derivative terms. Unfortunately solving elastic regularization potentials lead to a high computational effort. Second order regularisation has been investigated by Rueckert et al .[7] However the regularization is done just on a coarse grid and the flow field is penalized in a squared term which might not be optimal.

In this work we derive an optical flow based 3D volume registration method using a novel regularization prior that does not penalize locally affine deformations. Our regularization is based on second order derivatives, which leads to a substantial increase in computational complexity. However, we will show that our method is especially suited for an efficient parallel implementation on a consumer graphics processing unit (GPU). We also present an experimental setup where we apply our novel method to different medical volume data sets of the heart and the thorax. We compare our method to the curvarture registration approach[4] and a robust optical flow method using first order derivatives.

2. DEFORMABLE REGISTRATION ALGORITHM

2.1. Classical Optical Flow Model of Horn and Schunk

Horn and Schunk[5] pioneered in formulating the optical flow problem in a variational framework. For 3D images it is given as the minimizer of the following energy:

$$\min_{\boldsymbol{u}} \left\{ \int_{\Omega} \sum_{i=1}^{3} |\nabla u_i|^2 \; d\Omega + \lambda \int_{\Omega} \left(I_1 \left(\boldsymbol{x} + \boldsymbol{u}(\mathbf{x}) \right) - I_0 \left(\boldsymbol{x} \right) \right)^2 d\Omega \right\} \tag{1}$$

I_0 and I_1 are fixed and moving input image given in the domain $\Omega \subset \mathbb{R}^3$. $\boldsymbol{u} = \left(u_1 \left(\boldsymbol{x} \right), u_2 \left(\boldsymbol{x} \right), u_3 \left(\boldsymbol{x} \right) \right)^T$ is the three-dimensional displacement field and λ is a free weighting parameter, steering the relative importance of the two terms. The first (regularization) term penalizes variations in $\boldsymbol{u}$ in order to obtain smooth displacement fields. To overcome this restriction by allowing discontinuities in the displacement field, one can use robust regularization, e.g., Total Variation (TV).[6] The second (data) term represents the optical flow constraint, which implies that intensity values of I_0 do not change when moving to $I_1 \left(\boldsymbol{x} + \boldsymbol{u}(\mathbf{x}) \right)$ via the displacement $\boldsymbol{u}$. The quadratic error norm in the data term is not robust to violations of the optical flow constraint or non-Gaussian noise. A common method to improve robustness is to use, e.g., an L^1 norm instead.

2.2. Optical Flow Based on Second-Order Regularization

As outlined in the introduction, TV based flow regularization incurs a bias towards physically improbable flow fields. To overcome this drawback, we derive an operator $\diamond$ based on second order derivatives. It does not penalize affine deformations, since second derivatives of affine functions are zero. However, one has to be careful since second-order derivative operators in the three coordinate directions are not orthogonal and the local information of orientation and shape is entangled. Therefore, penalizing each of them, e.g., using the Euclidean vector norm, would induce a bias in the sense that certain affine deformation fields would be energetically favored.

Danielsson *et al.*[8] proposed a new operator to overcome this problem. They used circular harmonic functions to map the second order derivatives into an orthogonal space. In three spatial dimensions, the new operator is given by:

$$\diamond = \begin{pmatrix} \sqrt{\frac{1}{6}} \left(\frac{\partial^2}{\partial_x^2} + \frac{\partial^2}{\partial_y^2} + \frac{\partial^2}{\partial_z^2} \right) \\ -\sqrt{\frac{5}{24}} \left(\frac{\partial^2}{\partial_x^2} + \frac{\partial^2}{\partial_y^2} \right) + \sqrt{\frac{5}{6}} \frac{\partial^2}{\partial_z^2} \\ \sqrt{\frac{5}{8}} \left(\frac{\partial^2}{\partial_x^2} - \frac{\partial^2}{\partial_y^2} \right) \\ \sqrt{\frac{5}{2}} \frac{\partial^2}{\partial_x \partial_y} \\ \sqrt{\frac{5}{2}} \frac{\partial^2}{\partial_x \partial_z} \\ \sqrt{\frac{5}{2}} \frac{\partial^2}{\partial_y \partial_z} \end{pmatrix} \tag{2}$$

We adopt the operator $\diamond$ to regularize the 3D displacement field using the Euclidean vector norm of $\diamond u$.

$$||\diamond|| = \sqrt{\frac{1}{6}\left(\frac{\partial^2}{\partial_x^2} + \frac{\partial^2}{\partial_y^2} + \frac{\partial^2}{\partial_z^2} \right)^2 + \left(\sqrt{\frac{5}{24}}\left(\frac{\partial^2}{\partial_x^2} + \frac{\partial^2}{\partial_y^2} \right) + \sqrt{\frac{5}{6}} \frac{\partial^2}{\partial_z^2} \right)^2 + \frac{5}{8}\left(\frac{\partial^2}{\partial_x^2} - \frac{\partial^2}{\partial_y^2} \right)^2 + \frac{5}{2}\left(\left(\frac{\partial^2}{\partial_x \partial_y} \right)^2 + \left(\frac{\partial^2}{\partial_x \partial_z} \right)^2 + \left(\frac{\partial^2}{\partial_y \partial_z} \right)^2 \right)}$$

We combine this regularization term with a robust L^1 data term depicting the optical flow constraint with the Taylor approximation of the image residual $\phi(\boldsymbol{u}) = I_1(\boldsymbol{x} + \boldsymbol{u}_0) + \langle \boldsymbol{u} - \boldsymbol{u}_0, \nabla I_1 \rangle - I_0$ where $\boldsymbol{u}_0$ is an initial solution. The resulting optical flow model is given by:

$$\min_{\boldsymbol{u}} \left\{ \sum_{i=1}^{3} \int_{\Omega} \| \diamond u_i \| \, d\Omega + \lambda \int_{\Omega} |\phi(\boldsymbol{u})| \; d\Omega \right\} \tag{3}$$

After Taylor approximation the model becomes convex, such that a global minimizer on the domain of continuous displacement fields $\boldsymbol{u}$ can be computed. However, it has to be embedded into an iterative warping procedure to take the image non-linearity into account.

2.3. Numerical Solution

Solving the proposed optical flow model is an extension to our work proposed in.[9] Due to limited space, we have to omit the detailed derivation and its proof here. For the numerical procedure we introduce an additional variable $\boldsymbol{v} = (v_1, v_2, v_3)$ and propose the following minimization procedure:

$$\min_{\boldsymbol{u}} \left\{ \sum_{i=1}^{3} \int_{\Omega} \parallel \diamond u_i \parallel d\Omega + \frac{1}{2\theta} \sum_{i=1}^{3} \int_{\Omega} (u_i - v_i)^2 d\Omega + \lambda \int_{\Omega} |\phi(\boldsymbol{v})| \, d\Omega \right\} \tag{4}$$

This minimization procedure can be solved using an iteration scheme that alternately minimizes $\boldsymbol{u}$ and $\boldsymbol{v}$. The optimization for $\boldsymbol{u}$ uses a numerical algorithm based on a dual formulation to cope with the non-differentiability of the L^1 norm at zero.[10] Minimization of $\boldsymbol{v}$ can be reduced to a one-dimensional problem and implemented as a simple thresholding scheme. Both of these steps are perfectly suited for a parallel implementation using a GPU.

We implemented the numerical minimization procedure in part on the CPU and on a GPU using the CUDA framework.[11] Due to the image non-linearity in (4), we embed the numerical solution of the convex functional 4 in a multi-resolution scheme. This way the optical flow model can cope with large displacements. We build a Gaussian image pyramid on the GPU by successively smoothing and down-sampling the input images by a factor of 2. On each pyramid level, we solve (4) using the alternate optimization scheme, starting with the coarsest level and propagating displacement field solutions to the next finer level. We initialize $\boldsymbol{u}$ on the coarsest level with $\boldsymbol{u} = \boldsymbol{0}$. Our numerical scheme for each pyramid level is:

1. For fixed $\boldsymbol{v}$ solve the following functional in $\boldsymbol{u}$:

$$\min_{\boldsymbol{u}} \left\{ \sum_{i=1}^{3} \int_{\Omega} \parallel \diamond u_i \parallel d\Omega + \frac{1}{2\theta} \sum_{i=1}^{3} \int_{\Omega} (u_i - v_i)^2 d\Omega \right\} \tag{5}$$

2. For fixed $\boldsymbol{u}$ solve this functional for $\boldsymbol{v}$:

$$\min_{\boldsymbol{v}} \left\{ \frac{1}{2\theta} \sum_{i=1}^{3} \int_{\Omega} (u_i - v_i)^2 d\Omega + \lambda \int_{\Omega} |\phi(\boldsymbol{v})| \, d\Omega \right\} \tag{6}$$

2.4. Solution of $\boldsymbol{u}$

For solving equation 6 the dual variable $\boldsymbol{p}$, as suggested by T. Chan, G. Golub, and P. Mulet,[12] is introduced.

$$||\diamond \boldsymbol{u}|| = \max \{ \boldsymbol{p} \diamond \boldsymbol{u} \; : \; ||\boldsymbol{p}|| \leq 1 \} \tag{7}$$

where $\boldsymbol{p} = (p_1, p_2, p_3)^T$ is the dual variable. The approach of J. Carter[13] is used for further assumptions. Replacing $||\diamond \boldsymbol{u}||$ with the dual formation we get the following functional:

$$\min_{\boldsymbol{u}} \max_{||\boldsymbol{p}|| \leq 1} \underbrace{\left\{ \int_{\Omega} \boldsymbol{p} \diamond \boldsymbol{u} + \frac{1}{2\theta} \int_{\Omega} (\boldsymbol{u} - \boldsymbol{v})^2 \; d\Omega \right\}}_{\Psi(\boldsymbol{u}, \boldsymbol{p})} \tag{8}$$

We can interchange the *min* and *max* due to the facts:

1. The dual variable $\{\boldsymbol{p} : ||\boldsymbol{p}|| \leq 1\}$ is bounded.
2. The functional $\Psi(\boldsymbol{u}, \boldsymbol{p})$ in equation 8 is convex.

The obtained functional is:

$$\max_{||\boldsymbol{p}||\leq 1} \min_{\boldsymbol{u}} \underbrace{\left\{ \int_{\Omega} \boldsymbol{p} \diamond \boldsymbol{u} + \frac{1}{2\theta} \int_{\Omega} (\boldsymbol{u} - \boldsymbol{v})^2 \, d\Omega \right\}}_{\Psi(\boldsymbol{u},\boldsymbol{p})} \tag{9}$$

Chambolle showed in[10] that for a linear operator in the discrete domain the following assumption is valid:

$$\int_{\Omega} \boldsymbol{p} \diamond \boldsymbol{u} = \int_{\Omega} \diamond \boldsymbol{p} \, \boldsymbol{u} \tag{10}$$

The functional in equation 8 is changing to:

$$\max_{||\boldsymbol{p}||\leq 1} \min_{\boldsymbol{u}} \underbrace{\left\{ \int_{\Omega} \diamond \boldsymbol{p} \, \boldsymbol{u} + \frac{1}{2\theta} \int_{\Omega} (\boldsymbol{u} - \boldsymbol{v})^2 \, d\Omega \right\}}_{\Psi(\boldsymbol{u},\boldsymbol{p})} \tag{11}$$

$\Psi(\boldsymbol{u}, \boldsymbol{p})$ is strictly convex in the primal variable $\boldsymbol{u}$. Therefore $\boldsymbol{u}$ can be written as a function $\boldsymbol{v}$ by solving the first-order condition:

$$\nabla \Psi(\boldsymbol{u}, \boldsymbol{p}) = 0 \quad \Longleftrightarrow \quad \boldsymbol{u} = \boldsymbol{v} - \theta \diamond \boldsymbol{p} \tag{12}$$

Now, the functional can be formed without the primal variable $\boldsymbol{u}$:

$$\max_{||\boldsymbol{p}||\leq 1} \underbrace{\left\{ \int_{\Omega} \diamond \boldsymbol{p} \, (\boldsymbol{v} - \theta \diamond \boldsymbol{p}) + \frac{1}{2\theta} \int_{\Omega} (-\theta \diamond \boldsymbol{p})^2 \, d\Omega \right\}}_{\Gamma(\boldsymbol{u})} \tag{13}$$

We can form a minimization functional out of the previous by changing the algebraic sign:

$$\min_{||\boldsymbol{p}||\leq 1} \left\{ - \int_{\Omega} \diamond \boldsymbol{p} \, \boldsymbol{v} + \frac{\theta}{2} (\diamond \boldsymbol{p})^2 \, d\Omega \right\} \tag{14}$$

Using the formulation of Equation 4.15 we get the functional shown in[14]:

$$\min_{||\boldsymbol{p}||\leq 1} \left\{ - \int_{\Omega} \boldsymbol{p} \diamond \boldsymbol{v} + \frac{\theta}{2} (\diamond \boldsymbol{p})^2 \, d\Omega \right\} \tag{15}$$

The Euler Lagrange equation of the variational functional is:

$$- \diamond (\boldsymbol{v} - \theta \diamond \boldsymbol{p}) = 0 \qquad ||\boldsymbol{p}|| \leq 1 \tag{16}$$

The solution can be obtained by a gradient descent approach. A gradient descent step is defined as:

$$\widetilde{\boldsymbol{p}}^{k+1} = \widetilde{\boldsymbol{p}}^{k} + \frac{\tau}{\theta} [\diamond (\boldsymbol{v} - \theta \diamond \boldsymbol{p})] \tag{17}$$

The reprojection of the dual variable $\boldsymbol{p}$ is given by:

$$\boldsymbol{p}^{k+1} = \frac{\widetilde{\boldsymbol{p}}^{k+1}}{\max \left\{ 1, \left| \left| \widetilde{\boldsymbol{p}}^{k+1} \right| \right| \right\}} \tag{18}$$

2.5. Solution of $\boldsymbol{v}$

The Euler Lagrange equation of Equation 6 is:

$$\boldsymbol{v} - \boldsymbol{u} + \lambda\theta \frac{\phi(\boldsymbol{v})}{|\phi(\boldsymbol{v})|} \nabla I_1 = 0 \tag{19}$$

where the first order image residual $\phi(\boldsymbol{v})$ is defined as:

$$\phi(\boldsymbol{v}) = I_1(\boldsymbol{x} + \boldsymbol{u}_0) + \langle \boldsymbol{v} - \boldsymbol{u}_0, \nabla I_1 \rangle - I_0 \tag{20}$$

The image residual is just valid for small variations of $\boldsymbol{u}$ and $\boldsymbol{v}$. Another problem arises when $|\phi(\boldsymbol{v})|$ vanishes. To overcome these problems the following thresholding schema is applied:

$$\boldsymbol{v} = \boldsymbol{u} + \begin{cases} \lambda\,\theta\,\nabla I_1 & \text{if} \quad \phi(\boldsymbol{u}) < -\lambda\,\theta\,|\nabla I_1|^2 \\ -\lambda\,\theta\,\nabla I_1 & \text{if} \quad \phi(\boldsymbol{u}) > \lambda\,\theta\,|\nabla I_1|^2 \\ \phi(\boldsymbol{u})\nabla I_1 / |\nabla I_1|^2 & \text{if} \quad |\phi(\boldsymbol{u})| \leq \lambda\,\theta\,|\nabla I_1|^2 \end{cases} \tag{21}$$

Hereby the image residual $\phi(\boldsymbol{v})$ is allowed to vanish if the step from $\boldsymbol{u}$ to $\boldsymbol{v}$ is sufficiently small. Otherwise $\boldsymbol{v}$ makes a bounded step from $\boldsymbol{u}$ to decrease the magnitude of the residual $\phi(\boldsymbol{v})$.

3. EXPERIMENTAL RESULTS

We implemented our method on the TESLA C1060 Computing Processor (GPU) using the CUDA 2.0 framework.[11] All of our experiments were performed on an Intel 2.66 GHz Quad Core2-Duo machine with 4 GB RAM and the TESLA GPU under a 64-bit Linux operating system. Due to the 4GB GPU memory available on the TESLA GPU, we are able to process volumes of size 256^3 which require 3 GB of graphics memory. The runtime of our algorithm is approximately 9 minutes for this volume size when performing 100 iterations on the finest level of the image pyramid. We performed experiments using synthetically transformed and real clinical data sets and show in this section our quantitative and qualitative results on the algorithm performance in comparison with state-of-the-art methods.

3.1. Synthetic Data

Our synthetic experiments use a thoracic CT data set with a voxel size of 256^3 and $1.6mm$ isotropic physical resolution. Our data set comes from the NLM data collection project *. We simulated a breathing motion and added both, Gaussian and salt-and-pepper noise to the fixed and moving input images.

We performed six experiments. In Experiment A we added Gaussian noise (10%). In Experiments B, C, D, E and F we added 2%, 3%, 5%, 6%, 7% salt-and-pepper noise, respectively, and in Experiment G we added gaussian (10%) and salt-and-pepper (5%) noise. For quantitative evaluation we calculate the mean and standard deviation of the computed displacement field $\boldsymbol{u}$ versus the ground-truth displacement field. The results on the mean difference of synthetic and ground truth displacement fields are shown in Table 1.

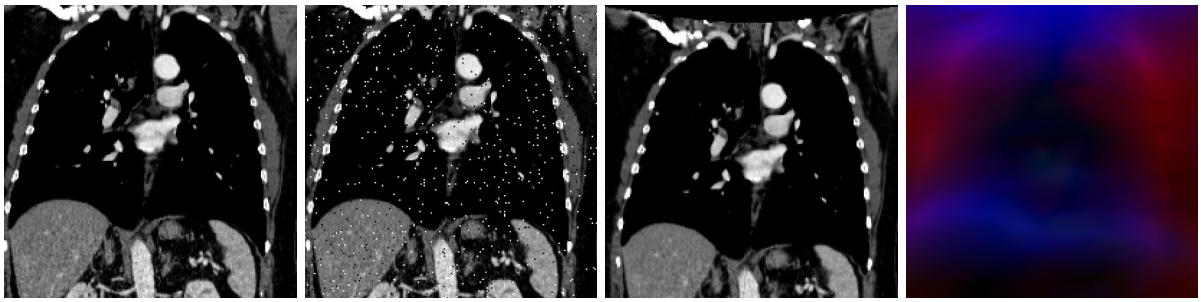

a) b) c) d)

Figure 1. a) Original data set. b) Original data set with 5% salt-and-pepper noise. c) Simulated diaphragm motion. d) Estimated motion by our second order method under 5% salt-and-pepper noise. Flow field magnitudes are represented in RGB space.

*http://nova.nlm.nih.gov

Measures		w/o noise	A	B	C	D	E	F	G
curvature	[mm]	2.936	3.175	3.323	3.474	3.522	3.382	3.915	3.902
first order	[mm]	2.689	2.805	2.781	2.856	2.932	3.095	3.197	3.063
second order	[mm]	**2.351**	**2.482**	**2.496**	**2.561**	**2.653**	**2.751**	**2.858**	**2.806**

Table 1. Quantitative evaluation of the synthetic experiments. We show the mean difference of the resulting displacement field compared with the ground truth displacement field.

3.2. Clinical Data

We also applied our algorithm to clinical data sets. Clearly, for clinical data there is no ground-truth displacement field available to compare to. It is solely possible to calculate similarity measures on the image intensities before and after registration. We calculate the root mean squared error of the intensity values (RMS) and the increase of [0, 1]-normalized mutual information (NMI) before and after registration. Our first experiment consisted of breathing motion compensation of two thoracic CT data sets, again taken from the NLM data collection project *. In our second experiment we used three 4D CT cardiac data series from the OsiriX project †. From each of these cardiac series we picked one volume around the peak-systole and the other around the end-diastole of the beating cycle. Every volume was resampled to an isotropic resolution ($1.6mm$ for the thoracic and $0.8mm$ for the cardiac data) with a voxel size of 256^3. To set up our algorithm we used $\lambda = 30$ for the thoracic and $\lambda = 60$ for the cardiac data. These λ values were determined empirically by testing several settings. Convergence was achieved after approximately 20 minutes for both types of data sets.

We again compare our method to the curvature registration approach and a first order optical flow method. The quantitative results of our experiment are given in Figure 2 and some qualitative results are shown in Fig. 4. Our method shows the overall best performance over all experiments compared to the other methods.

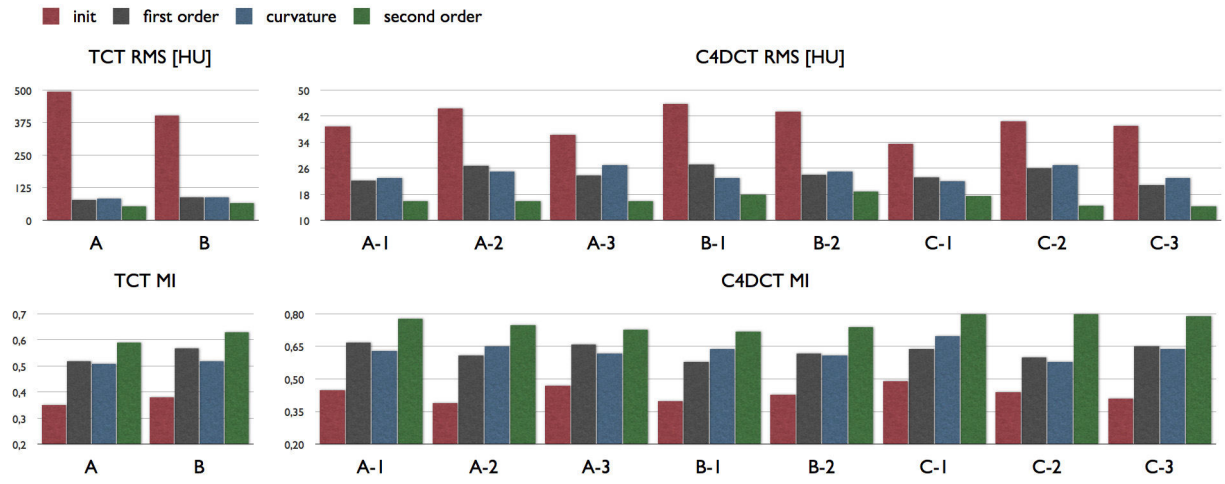

Figure 2. Quantitative evaluation of the clinical data sets using RMS and [0-1]-normalized mutual information (NMI) of the intensities.

4. CONCLUSION

In this work a second order regularization method using a novel regularization prior for deformable optical flow based image registration was presented. We have shown that the numerical implementation of this model can be efficiently performed using current consumer GPUs as massively parallel numerical co-processors. Our experiments on synthetic and clinical thorax and heart CT data has confirmed that our method behaves very

†http://pubimage.hcuge.ch:8080

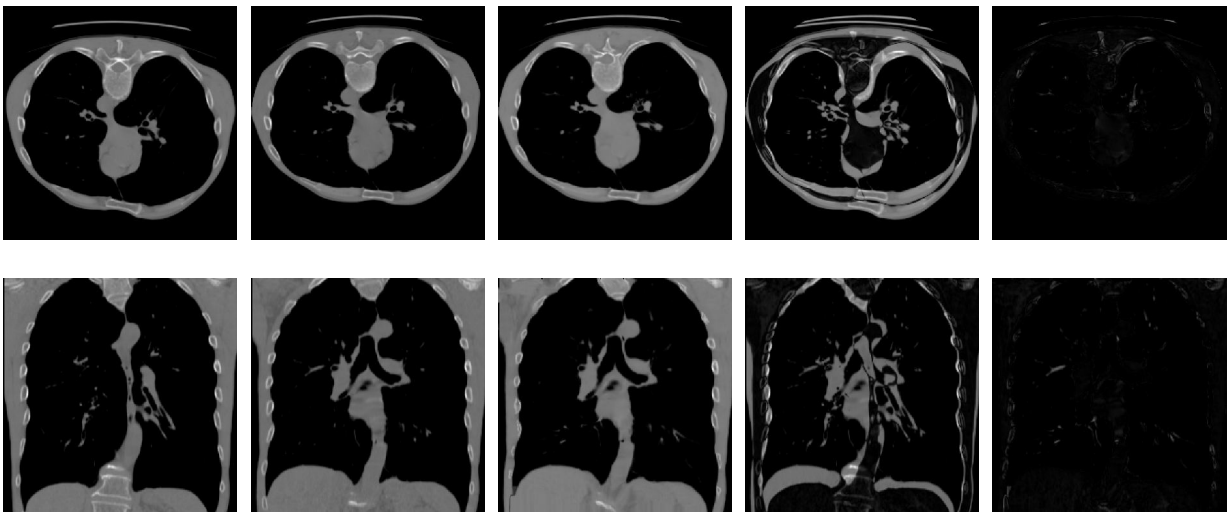

a) b) c) d) e)

Figure 3. Qualitative results on thoracic CT data sets. a) moving image $I_M(\boldsymbol{x})$. b) fixed image $I_F(\boldsymbol{x})$. c) warped image $I_M(\boldsymbol{x}+\boldsymbol{u})$. d) difference image before registration $|I_F(\boldsymbol{x}) - I_M(\boldsymbol{x})|$. e) difference image after registration $|I_F(\boldsymbol{x}) - I_M(\boldsymbol{x}+\boldsymbol{u})|$.

well in practical deformable registration applications. Further work has to be done to validate our claims on a larger number of data sets and using more sophisticated synthetic deformation models. A comparison to an implementation of elastic registration is also planned in future. From a practical point of view we will investigate how to further improve the runtime of the method. From the theoretical side we will investigate the relation of the higher-order Total Variation models to explicitly modeled spline-based methods[7] as discussed in.[15]

REFERENCES

1. J. B. A. Maintz and M. A. Viergever, "A Survey of Medical Image Registration," *Medical Image Analysis* **2**(1), pp. 1–36, 1998.
2. W. R. Crum, T. Hartkens, and D. L. G. Hill, "Non-rigid image registration: Theory and Practice," *The British Journal of Radiology - Imaging Processing Special Issue* **77**, pp. S140–S153, December 2004.
3. R. Bajcsy and S. Kovacic, "Multiresolution Elastic Matching," *Computer Vision, Graphics and Image Processing* **46**(1), pp. 1–21, 1989.
4. J.-P. Thirion, "Image matching as a diffusion Process: An analogy with Maxwell's demons," *Medical Image Analysis* **2**(3), pp. 243–260, 1998.
5. B. K. P. Horn and B. G. Schunck, "Determining optical flow," *Artificial Intelligence* **17**(1-3), pp. 185–203, 1981.
6. T. Pock, M. Urschler, C. Zach, R. Beichel, and H. Bischof, "A duality based algorithm for TV-L1-optical-flow image registration," in *Proc Int Conf Med Image Comput Comput Assist Interv (MICCAI 2007)*, pp. 511–518, 2007.
7. D. Rueckert, L. I. Sonoda, C. Hayes, D. L. G. Hill, M. O. Leach, and D. J. Hawkes, "Nonrigid Registration Using Free-Form Deformations: Application to Breast MR Images," *IEEE Transactions on Medical Imaging* **18**, pp. 712–721, August 1999.
8. P.-E. Danielsson and Q. Lin, "Efficient detection of second-degree variations in 2D and 3D images," *Journal of Visual Comm. and Image Representation* **12**, pp. 255–305, 2001.
9. "Self Reference," -.

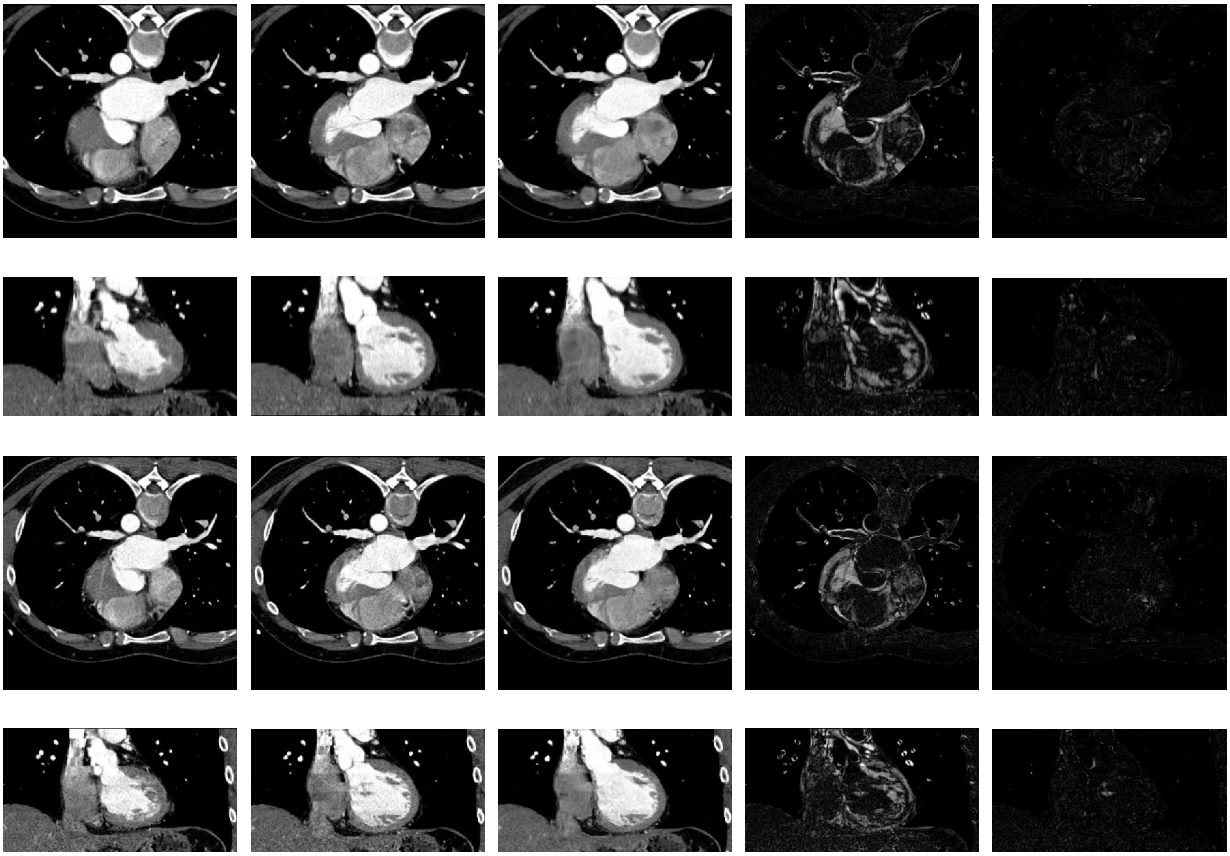

a) b) c) d) e)

Figure 4. Qualitative results on 4D cardiac CT data sets. a) moving image $I_M(\boldsymbol{x})$. b) fixed image $I_F(\boldsymbol{x})$. c) warped image $I_M(\boldsymbol{x}+\boldsymbol{u})$. d) difference image before registration $|I_F(\boldsymbol{x}) - I_M(\boldsymbol{x})|$. e) difference image after registration $|I_F(\boldsymbol{x}) - I_M(\boldsymbol{x}+\boldsymbol{u})|$.

10. A. Chambolle, "An algorithm for total variation minimization and applications," *Journal of Mathematical Imaging and Vision* **20**, pp. 89–97, 2004.
11. NVidia, "NVidia CUDA Compute Unified Device Architecture programming guide 2.0," tech. rep., NVIDA Corp., Santa Clara, CA, USA, 2008.
12. T. Chan, G. Golub, and P. Mulet, "A nonlinear primal- dual method for total variation-based image restoration," in *SIAM J. Sci. Comp., Computational and Applied Mathematics Report* **20**, pp. 1964–1977, September 1999.
13. J. L. Carter, *Dual Methods for Total Variation-Based Image Restoration.* PhD thesis, University of California, Los Angeles, 2001.
14. W. Trobin, T. Pock, D. Cremers, and H. Bischof, "An unbiased second-order prior for high-accuracy motion estimation," in *DAGM Symposium on Pattern Recognition*, G. Rigoll, ed., **30**, pp. 396–405, Springer, June 2008.
15. G. Steidl, S. Didas, and J. Neumann, "Splines in higher order TV regularization," *International Journal of Computer Vision* **70**(3), pp. 241–255, 2006.